

From Jekyll to Hyde and Beyond: Hydrogen's Multifaceted Role in Passivation, H-Induced Breakdown, and Charging of Amorphous Silicon Nitride

Jonathon Cottom, Lukas Hückmann, Emilia Olsson, and Jörg Meyer*




Cite This: *J. Phys. Chem. Lett.* 2024, 15, 840–848



Read Online

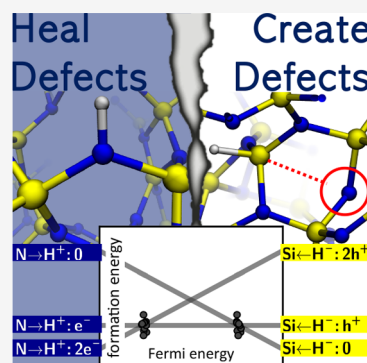
ACCESS |

 Metrics & More

 Article Recommendations

 Supporting Information

ABSTRACT: In semiconductor devices, hydrogen has traditionally been viewed as a panacea for defects, being adept at neutralizing dangling bonds and consequently purging the related states from the band gap. With amorphous silicon nitride ($a\text{-Si}_3\text{N}_4$)—a material critical for electronic, optical, and mechanical applications—this belief holds true as hydrogen passivates both silicon and nitrogen dangling bonds. However, there is more to the story. Our density functional theory calculations unveil hydrogen's multifaceted role upon incorporation in $a\text{-Si}_3\text{N}_4$. On the “Jekyll” side, hydrogen atoms are indeed restorative, healing coordination defects in $a\text{-Si}_3\text{N}_4$. However, “Hyde” emerges as hydrogen induces Si–N bond breaking, particularly in strained regions of the amorphous network. Beyond these dual roles, our study reveals an intricate balance between hydrogen defect centers and intrinsic charge traps that already exist in pristine $a\text{-Si}_3\text{N}_4$: the excess charges provided by the H atoms result in charging of the $a\text{-Si}_3\text{N}_4$ dielectric layer.



Silicon nitride has been a technologically important material for a number of years due in no small part to its attractive chemical, mechanical, and electronic properties. This has led to it being deployed in a broad range of applications covering wear-resistant coatings,¹ electronic devices (MOSFETs and MEMS),^{2,3} high-energy optics,^{4–6} integrated photonics,^{7,8} and lithography.^{9–11} For a small number of applications, silicon nitride is used in the crystalline phase.^{12,13} However, in most use cases it is deployed as an amorphous thin film ($a\text{-Si}_3\text{N}_4$).^{3,14–19} The addition of hydrogen can be intentional, as is the case with photovoltaics and electronic devices that undergo a H-anneal step. This passivation step has been shown to be both a blessing, passivating dangling bonds,^{20–22} and a curse, affecting structural stability and altering the charge trapping properties.^{23–26} Alternatively, H can be incorporated unintentionally as a result of exposure to the environment, such as is the case in lithography.^{4–6,9–11,27} Finally, a certain concentration of H will be incorporated from the precursors during thin film growth by chemical vapor deposition, typically SiH_4 and its derivatives. Regardless of how H is introduced to $a\text{-Si}_3\text{N}_4$, at the atomic scale an understanding of H incorporation and the concomitant modification of the material's properties has not been established.

Notwithstanding, experimental and theoretical studies have provided a number of important insights. H defects have been linked to the passivation of dangling bonds within the $a\text{-Si}_3\text{N}_4$ network,^{20–22,28–38} based on a reduction of the observed concentration of paramagnetic centers upon increases in Si–H vs N–H concentration.^{39,40} This reduction in undercoordinated Si and N has additionally been linked to the observed increase in

breakdown strength and perhaps surprisingly to a decrease in the $a\text{-Si}_3\text{N}_4$ film's tensile stress.²³ In addition, the post-deposition treatment with H leads to significant changes in the observed photoluminescence and EPR spectra.^{26,41,42} The latter results suggest that H plays a dual role, leading to a reduction in midgap recombination centers while favoring or introducing others, resulting in both radiative and nonradiative recombination pathways.²⁶ Conversely, it has been observed that as the H concentration in the $a\text{-Si}_3\text{N}_4$ film increases, the temperature stability of the film decreases.^{24,25,43,44} The disparate nature of H incorporation with respect to the properties of $a\text{-Si}_3\text{N}_4$ suggests a range of atomic environments to be of relevance, beyond just the passivation of dangling bonds.

H incorporation in a variety of wide band gap oxides has been extensively studied.^{45–54} Therefore, it is tempting to look for parallels between nitrides and oxides. In particular, the interaction of H with SiO_2 shows a number of similar trends as for $a\text{-Si}_3\text{N}_4$ summarized above, reducing the number of coordination defects while forming new defect centers.^{52–55} The formation of new defect centers and the disruption of the silica lattice are suggested to result in the observed hydrolytic weakening, whereby exposure to H_2 and H_2O induces a

Received: December 1, 2023

Revised: January 5, 2024

Accepted: January 9, 2024

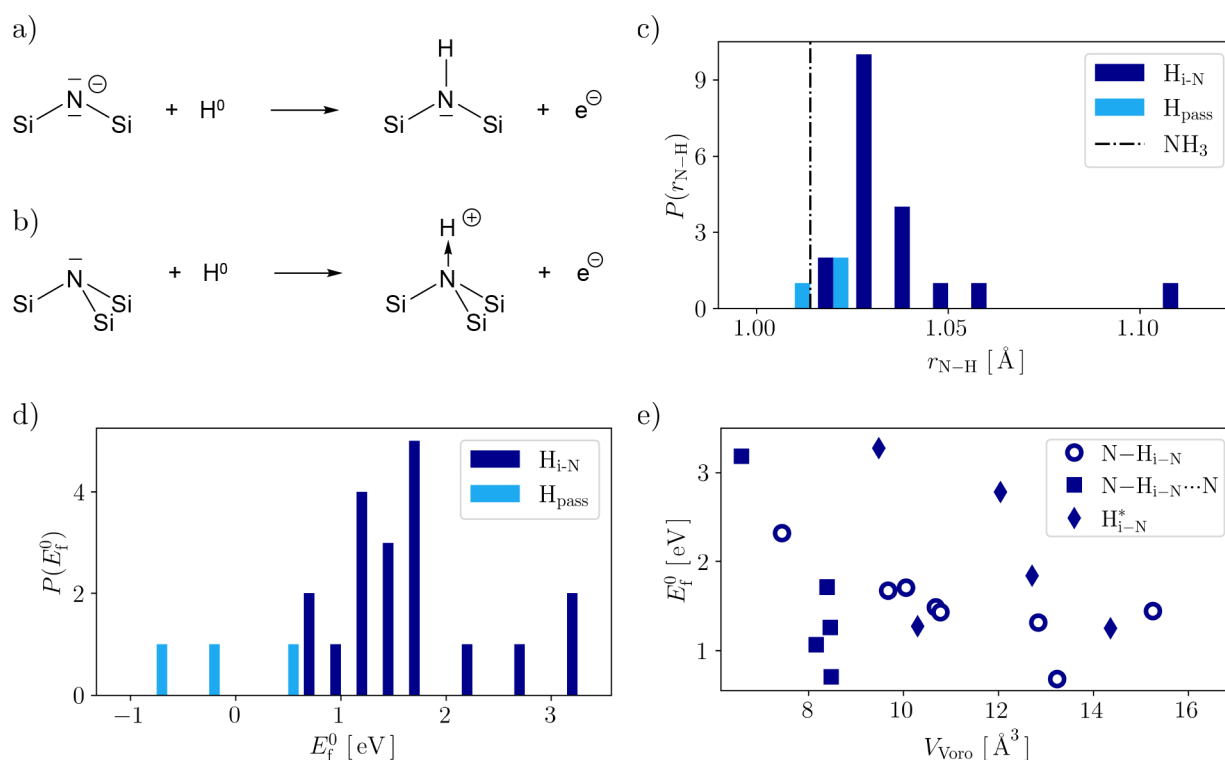


Figure 1. Schematic representation of N–H defect configurations on two- and three-coordinate host atoms forming a) H passivation sites (H_{pass}) and b) H interstitial sites (H_{i-N}) in the neutral charge state ($q = 0$). The excess electron of the neutral hydrogen atom (H^0) is detached from the site and trapped at an intrinsic defect in the material. c) Distribution P of the N–H bond lengths for H_{pass} (light blue) and H_{i-N} (dark blue). For comparison, the N–H bond length of ammonia (NH_3) is indicated as the dashed–dotted line.⁶⁰ d) Distribution P of the formation energies E_f^0 (same color code as in c). e) E_f^0 as a function of the Voronoi volume V_{Voro} for H_{i-N} . This group of defects is further decomposed into different subgroups: Interstitials with a hydrogen bridge-like site $N-H_{i-N}\cdots N$, which are marked as squares (28%). Those inducing new electron trap sites not present in the pristine cell (H_{i-N}^*) are marked as diamonds (23%). The remainder (49%), where H interacts with a single N and the electron is trapped at the original H-free trap site, are labeled by $N-H_{i-N}$ and marked as empty circles.

significant weakening in SiO_2 and $\alpha\text{-Si}_3\text{N}_4$.^{43,44,56,57} Theoretical studies have provided atomistic insights into H incorporation in SiO_2 and identified a mechanism for the H-induced bond breaking.^{52–55} In general, for a broad range of oxides, H defects fit into two main categories. The first category is amphoteric defects, which result in H states deep in the band gap that typically exhibit negative U character, whereby the charge state (+/–) is dictated by the Fermi energy in the device. Alternatively, H can act as an n-type dopant introducing states in the vicinity of the conduction band minimum (CBM). A link between the (+/–) H charge transition level (CTL) and a universal value has been postulated, which further is related to the charge neutrality level (3.0,⁴⁹ 3.9,⁵¹ and 4.5⁴⁸ eV below the vacuum level, depending on the electronic structure approach employed). Li and Robertson⁵¹ noted this description and the concomitant universal value breakdown when the H is able to form a dative bond with the O-site. Considering the fact that chemical bonding in $\alpha\text{-Si}_3\text{N}_4$ is markedly different compared to that in $\alpha\text{-SiO}_2$, it is an open question of whether (and if so how) the aforementioned prevalent description of H defects can be extended to this class of materials.

Here we present a systematic study of H incorporation in $\alpha\text{-Si}_3\text{N}_4$ as a function of the local atomic environment. To ensure that a statistically meaningful range of H incorporation sites are considered, we build on the sampling scheme developed in our previous work.⁵⁸ We study the stability, structural features, charging behavior, and interplay between the extrinsic H defects and intrinsic charge trapping as characterized before.⁵⁸ This

allows us to quantify the multifaceted role H plays in $\alpha\text{-Si}_3\text{N}_4$, including passivation and the hitherto unknown structural modifications and H-induced breakdown of the network. Our analysis underscores a pronounced interplay between H and existing charge traps within the amorphous network. Contrary to the role of H as either an amphoteric defect center or an n-type dopant, more typically encountered, this nuanced behavior finds its roots in semilocalized states proximate to the CBM and VBM, resulting in an electrically inactive H center. Upon the incorporation of charge, predominantly donated by hydrogen, the excess charge is then localized at intrinsic traps.

H Incorporation in $\beta\text{-Si}_3\text{N}_4$. As a starting point, we briefly revisit hydrogen incorporation in the most stable crystalline phase ($\beta\text{-Si}_3\text{N}_4$), which has been previously studied by Di Valentin et al.³³ and Grillo et al.⁵⁹ To facilitate the comparison with $\alpha\text{-Si}_3\text{N}_4$, we have performed calculations with our computational setup. Full details are included in the [Supporting Information](#), and a brief summary is given here: In $\beta\text{-Si}_3\text{N}_4$, hydrogen forms a negative- U ($U \approx -0.5$ eV) amphoteric defect familiar from a broad range of oxides,^{48,51} most notably SiO_2 . Depending upon the Fermi energy, either the H^+ or H^- is favored. At $E_F < 3.28$ eV, the H^+ is favored, sitting at a N site with an N–H separation of 1.05 Å. Above 3.28 eV, the H^- is favored, sitting adjacent to a Si with a separation of 1.5 Å. Finally, for the neutral charge, while never energetically favored, the H adopts an interstitial configuration. This maximizes the distance to the neighboring ions, resulting in a Si/N–H separation of 2.4 Å. The (+/–) CTL sits approximately 4.15 eV below the vacuum

level and is in reasonable agreement with the observations of van de Walle and Neugebauer⁴⁸ as well as Li and Robertson.⁵¹ Interestingly and in contrast to the crystalline system, the noninteracting H^0 interstitial does not form in a-Si₃N₄. Instead, both N- and Si-centered H defects are found and discussed below, starting from the neutral charge state in both cases.

N–H Defects. Two main types of N–H defects are dictated by the original coordination of the reference site in the precursor geometry (Figure 1a,b):

1. H incorporation on two-coordinate N resulting in a passivation-type interaction (Si_2N-H_{pass}), and
2. H incorporation on three-coordinate N resulting in a tetrahedral-like distortion of the planar N forming a hydrogen interstitial (Si_3N-H_{i-N}).

The N–H bond lengths for both cases sit in a tight range between 1.01 and 1.06 Å with one outlier at 1.10 Å and the mean at 1.03 Å (Figure 1c). This makes the bonds marginally elongated compared to the N–H bond length in ammonia.⁶⁰ As to be expected, the very few H_{pass} defects present in our cell form the closest match and also come with the most favorable formation energies as shown in Figure 1d. Again for both H_{pass} and H_{i-N} , incorporation coincides with negligible structural relaxation as the adjacent N–Si bonds lengthen only by 0.11 Å (~6%) on average. In contrast, the formation energies for H_{i-N} extend over a considerable range of 0.68 to 3.27 eV (see Figure 1d). The fact that the H_{i-N} sites are uniform in terms of the N–H bond length and coordination geometry of the N-host indicates that the local environment of the host site dictates E_f^0 . This is confirmed in Figure 1e, illustrating that E_f^0 scales with the local steric environment, described by the Voronoi volume (V_{Voro}) of the incorporation site. In general (empty circles), a high degree of steric crowding (small V_{Voro}) results in high E_f^0 , and a small degree of steric crowding (large V_{Voro}) results in low E_f^0 . Sites with a nitrogen atom opposite to the host atom lead to a bridge-like interaction (N–H···N). The H···N distance is between 1.68 and 1.85 Å with an N–H···N angle between 1.3 and 32.6°. These structural arrangements allow H incorporation in sterically crowded regions of the lattice with a reduced energetic penalty (filled squares in Figure 1e). Finally, a subset of H_{i-N} defects can be distinguished, creating new states for electron trapping that are not present in the pristine cell (*vide infra*). As illustrated by the filled diamonds in Figure 1e, this subset follows the aforementioned trend less clearly.

Consideration of the +1 and –1 charge states shows that the H geometry is decoupled from the charge state with no change in either the N–H bond length or orientation. The reason for this becomes apparent by considering the electronic density of states (DOS) in the neutral charge state as shown in Figure 2a for a representative configuration. The H-induced electronic states are smeared out, with no significant contributions to the DOS below the VBM and empty states ~1.0 eV above the CBM. As there are no H states within the band gap, H–N is electronically inactive, and the charge state of H is thus independent of the device Fermi level, unlike for amphoteric H defects. Instead, here H is datively bound to N, resulting in a H^+ . The excess electron provided by the hydrogen is localized at an intrinsic trap site previously identified and characterized (strained SiN₄ tetrahedra, see Figure 2b).⁵⁸ For the majority of cases (77%, given by N– H_{i-N} and N– $H_{i-N} \cdots N$ in Figure 1e), further examination of the spin density, Mulliken charge, and DOS in the same way as described in detail in our previous work⁵⁸ reveals an unpaired electron localizing consistently on

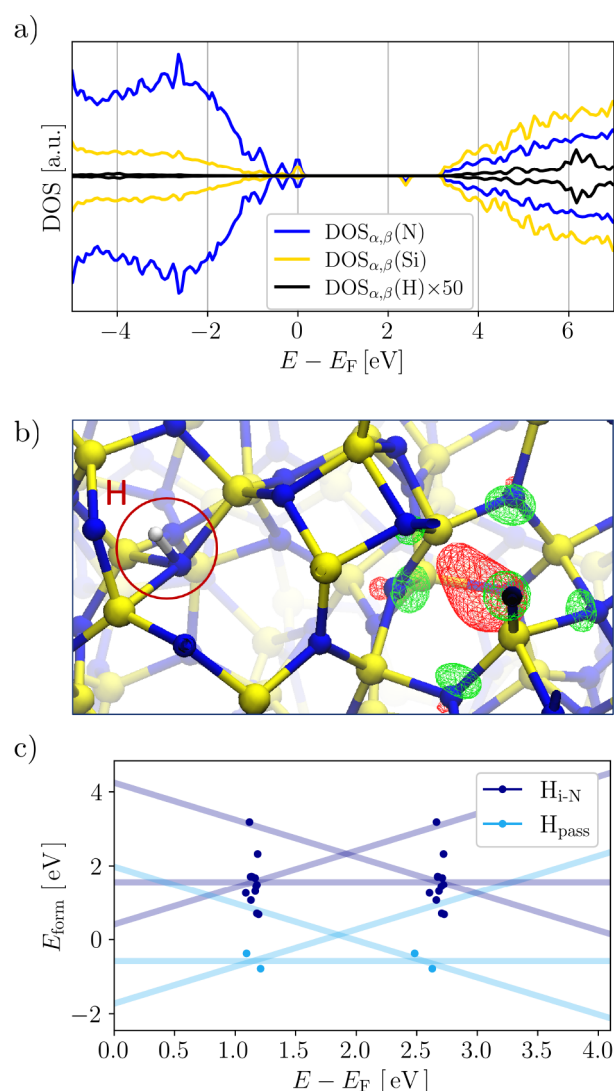


Figure 2. a) Projected electronic density of states (DOS) of Si (yellow), N (blue), and H (black) in a single representative neutral H_{i-N} configuration relative to the Fermi level E_F . The DOS of H is amplified by a factor of 50 for visibility. b) Representative example of the localized state on a Si atom formed independently from the N–H site in the neutral charge state. Si is colored yellow, N blue, and H white. The respective spin channels are colored red and green. c) Formation energies E_{form} as a function of the Fermi level E_F for the H_{pass} and H_{i-N} defects in the +1, neutral, and –1 charge states (same color code as in Figure 1f). Solid lines mark the average over the entire ensemble, and points indicate the individual +1/0 (average 1.2 eV) and 0/–1 (average 2.6 eV) charge transition levels. Samples inducing new electron trap sites not present in the pristine cell (H_{i-N}^* in Figure 1e) are not included.

the same intrinsic trap site in our simulation cell as illustrated in Figure 2b and Figure S3 in the Supporting Information. The fact that charge trapping is thus dominated by a feature of pristine a-Si₃N₄ rationalizes the lack of geometric relaxation of H defects upon charging and the extremely small spread of the CTLs shown in Figure 2c. Both are distinct features of H incorporation enabled by dative bonding and are clearly at odds with amphoteric H defects. In the remaining cases (23% H_{i-N}^* in Figure 1e, not considering H_{pass}), the structural distortion caused by the H incorporation induces an alternative precursor site, centered on a single distorted Si tetrahedron where the electron localizes. In both cases, this intimate link between

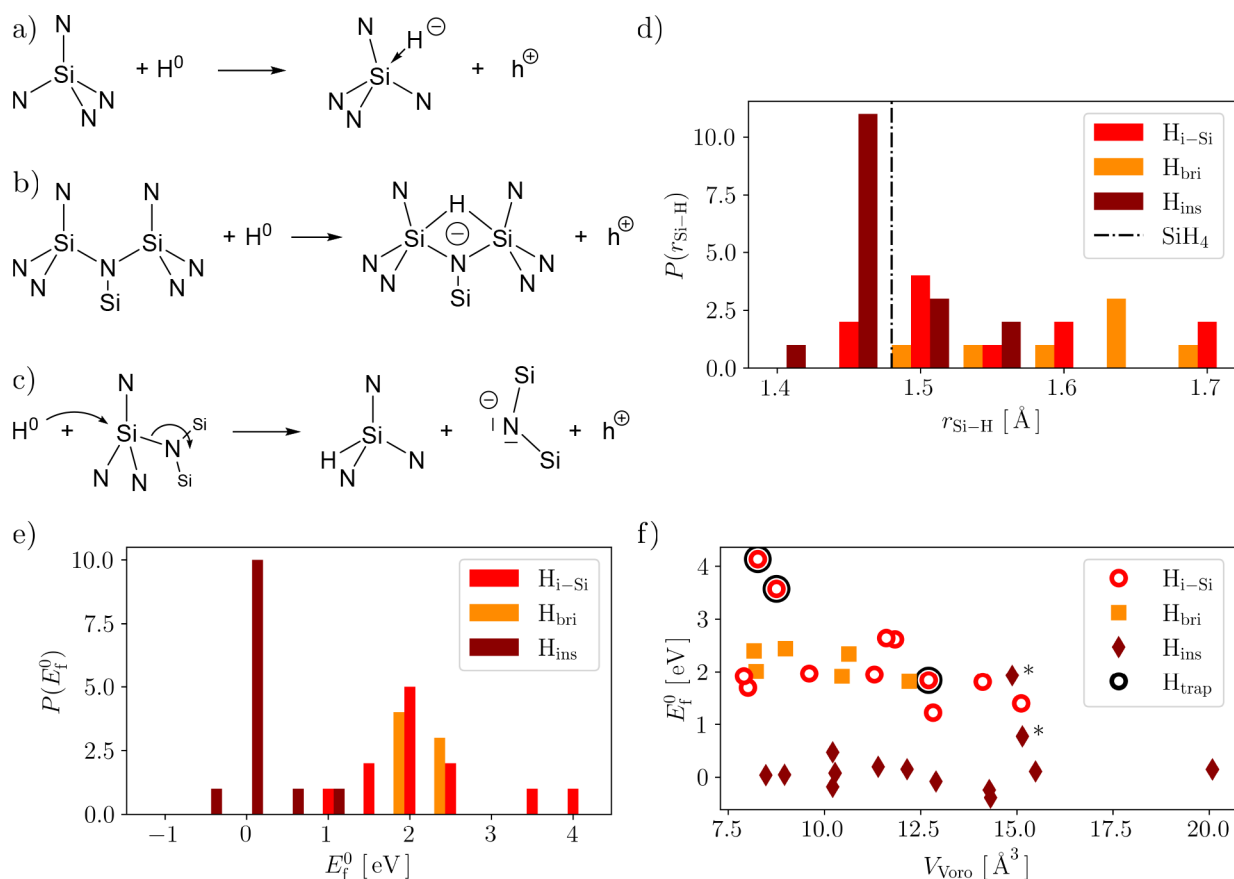


Figure 3. Schematic representation of Si–H defect configurations in the neutral charge state ($q = 0$) with a) H interstitial sites (H_{i-Si}), b) bridging H sites (H_{bri}), and c) H insertion sites (H_{ins}). The electron deficit to form a Si–H bond is compensated for by taking an electron from the valence band, inducing a hole polaron (h^+) at a site uncorrelated with the H defect. d) Distribution P of the Si–H bond length with H_{i-Si} (red), H_{bri} (orange), and H_{ins} configurations (dark red). For comparison, the Si–H bond length of silane (SiH_4) is indicated by the dashed–dotted line.⁶¹ e) Distribution P of the formation energies E_f^0 (the same color scheme as in d). f) E_f^0 as a function of the Voronoi volume V_{Voro} for the configurations H_{i-Si} (hollow circles), H_{bri} (squares), and H_{ins} (diamonds). There are three cases marked with black circles (H_{trap}), which have a notably different electronic structure causing H-induced trapping, as further discussed in the text.

(effectively) adding or removing charges and structural relaxation is equivalent to intrinsic charge trapping in the H-free cell. It is important to note that in the -1 charge state both electrons occupy the trap state, forming a bipolaron. This was not included in our previous study because only single electron/hole trapping was considered in the pristine cell.⁵⁸ The local structure of the trap site experiences pronounced relaxation, resulting in a breaking of the Si–N ($\Delta r_{SiN} = 0.55 \text{ \AA}$), and the Si is back-projected in such a way that it interacts with an adjacent Si neighbor. Nevertheless, the Si–Si distance is 2.26 \AA and the structure is similar to that of $N_3Si-SiN_{x \in \{3,4\}}$ previously described.⁵⁸

Si–H Defects. We have identified and schematically depicted three main classes of defects in Figure 3a–c:

1. H interacting with a single fully coordinated Si atom (N_4Si-H_{i-Si}),
2. H bridging two adjacent Si atoms, in addition to their regular link via a N atom in the $a-Si_3N_4$ network ($N_4Si-H_{bri}-SiN_4$), and
3. H inserting across a strained Si–N bond, resulting in $H-SiN_3$ and an adjacent two-coordinate N (N_3Si-H_{ins}).

The Si–H bond lengths spread over a range from 1.40 to 1.69 \AA (Figure 3d), with the H_{i-Si} and H_{bri} configurations being significantly elongated compared to the Si–H bond length in

silane (1.48 \AA).⁶¹ On average, they measure 1.53 and 1.59 \AA , respectively. The H_{bri} bonds are shifted to higher values as they are shared between adjacent Si atoms. In the H_{i-Si} and H_{bri} configurations, the coordination shell of the Si remains intact. In contrast, the H_{ins} sites show a dramatic elongation of one of the Si–N bonds with a mean separation of 2.75 \AA post relaxation, while the Si–H bond relaxes to 1.47 \AA on average, approximately the same length found in the silane (Figure 3d). The range of Si–H bond lengths is dictated by the local environment, impacting how the H is incorporated initially and subsequently how the defect center is able to relax. As schematically depicted in Figure 3c, H insertion occurs via backside insertion on the SiN_4 tetrahedra so that the opposing Si–N bond is broken while the Si-center back projects. The relaxation bears similarities to the “puckering” described for oxygen vacancies in $a-SiO_2$,^{55,62} albeit with some important differences as the relaxation drives the breaking of an Si–N bond and is restricted due to the lack of flexibility imparted by three-coordinate N-anions. This is in contrast to H-induced bond rupture found in SiO_2 where insertion is driven by interaction with the O site, resulting in the hydroxylated E’ center ($O_3Si-OH + SiO_3$).^{53,54}

In terms of formation energy E_f^0 , the Si–H defects extend over a wide range between -0.39 and 4.13 eV (Figure 3e). The energy range can be further grouped by the incorporation modes

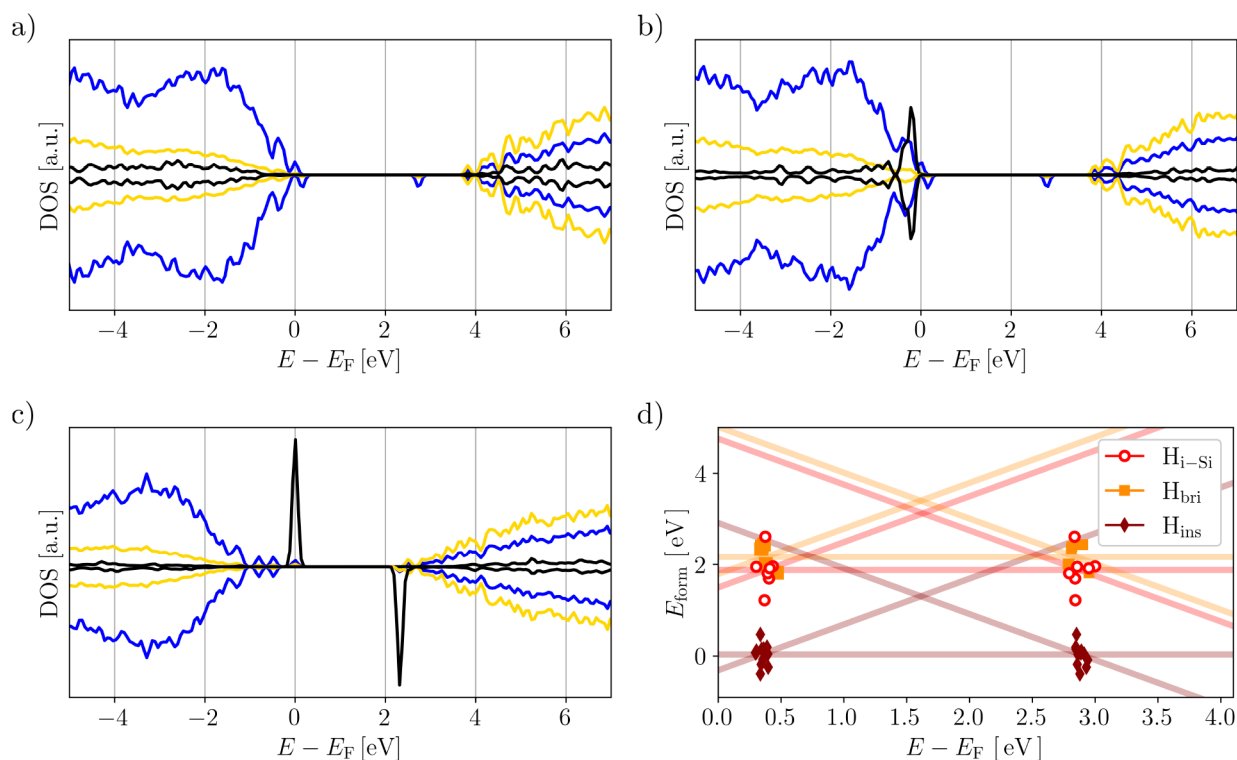


Figure 4. a–c) Projected electronic density of states (DOS) of Si (yellow), N (blue), and H (black) relative to the Fermi level E_F . The DOS of H is amplified by a factor of 50 for visibility. a) and b) show DOSs for individual configurations representative of H_{ins} and H_{bri} , respectively. c) The H_{i-Si} configuration shown here is exceptional, where no proper Si–H bond could be formed. This results in a single electron being localized on the H atom while not inducing a hole polaron in the bulk (as depicted in Figure 3a). d) Formation energies E_{form} as a function of the Fermi level E_F for the H_{i-Si} , H_{bri} , and H_{ins} defects in the +1, neutral, and –1 charge states (same color code as in Figure 3f). Solid lines mark the average over the entire ensemble together with the individual data points for the +1/0 (average 0.4 eV) and 0/–1 (average 2.9 eV) charge transition levels.

as shown in Figure 3e,f: analogous to interstitial sites centered on nitrogen, H_{i-Si} scales with the local steric environment (V_{Voro}), where regions with low steric repulsion (large V_{Voro}) are favored over sterically crowded regions (small V_{Voro}). Furthermore, in common with N–H centers, interaction with a neighboring Si atom results in stabilization of the H_{bri} configurations. It is interesting that there are two intermediate configurations identified, where the local environment frustrates the relaxation to H_{ins} , resulting in an H–SiN₃–N-type configuration (Figure 3f indicated with an asterisk). In addition and as indicated in Figure 3f by black circles, there are three H_{i-Si} -like cases that are electronically distinct, as further analyzed below. In contrast, for H_{ins} sites a different picture emerges: E_f^0 sits in a tight range between –0.39 and 0.77 eV with the mean at 0.11 eV, with a small number of outliers at higher energy where the local geometry frustrates the relaxation. E_f^0 is largely independent of the local steric environment, being driven by the H insertion.

Focusing on the majority of the Si–H configurations, the corresponding +1 and –1 charge states turn out to leave the H-incorporation geometry unchanged, just as observed for the N-centered H defects above. The reason for this is illustrated by the DOSs shown in Figure 4a,b) for H_{ins} and H_{bri} , respectively. The H states sit above the CBM (H_{ins}) and below the VBM (H_{bri}), resulting in an electrically inactive H center. The charge trapping in the system is mediated by h^+ trapping on two-coordinate N as previously described.⁵⁸ For H_{ins} , the formation of the Si–H and creation of the two-coordinate N⁰ results in the relaxation of the h^+ to the lowest-energy trap site. In H_{i-Si} and H_{bri} , the H is bound to one or more Si, resulting in a H^- (quantified by a Mulliken

charge of –0.1e) in line with the trend from the H^- -cation interaction observed in oxides. The formation of H^- is driven by the H states sitting below the VBM: The neutral charge state Si + H^0 yields Si ← H^- + h^+ after charge relaxation (where ← symbolizes dative bonding). In each case, the hole is localized on the same two-coordinate N, which was the previously identified hole trapping site in the H-free case. Analogous to the N centers, charge trapping is thus dominated by a feature of pristine a-Si₃N₄ and rationalizing the very small spread of the CTLs shown in Figure 4d as a consequence.

We now return to those H_{i-Si} configurations which are marked in Figure 3f by black circles. Based on their geometry, the H atom appears to interact with a single Si atom only in those cases. However, the representative DOS shown in Figure 4c and the charged counterparts of these configurations reveal something quite different, namely, that in all of those cases H-induced traps form. These traps are formally in the neutral charge state (H^0) with the frontier states being both H in nature. This is the reason that they show negative- U (close to $U = 0$ eV) behavior with a charge-dependent structural relaxation of the incorporated H atoms (more details in section 6 of the Supporting Information), as extensively described for amphoteric hydrogen defects in wide band gap oxides.

H incorporation in a-Si₃N₄ is rich and notably different from what has been previously described for crystalline β -Si₃N₄, where the formation of negative- U amphoteric defect centers dominates, as also seen in a broad range of wide band gap oxides. Table 1 provides a schematic overview for a-Si₃N₄, including its charge dependence, which we discuss further in the following.

Table 1. Simplified Schematic Overview of Charge Relaxation for Both N- and Si-Centered H Defects for Different (Global) Charge States q^a

q	N–H		Si–H	
	unrelaxed	relaxed	unrelaxed	relaxed
+1	$N + H^+$	$N \rightarrow H^+$	$Si + H^+$	$Si \leftarrow H^- + 2 h^+$
0	$N + H^0$	$N \rightarrow H^+ + e^-$	$Si + H^0$	$Si \leftarrow H^- + h^+$
-1	$N + H^-$	$N \rightarrow H^+ + 2 e^-$	$Si + H^-$	$Si \leftarrow H^-$

^aFor each defect center, the two subcolumns describe the unrelaxed and relaxed charge configurations. For the latter, e^- denotes an intrinsic electron polaron, and h^+ denotes an intrinsic hole trap. The N/Si–H bonds are presented as dative bonds (\rightarrow/\leftarrow) to describe the rearrangement of electrons upon H incorporation.

In agreement with previous work,^{33,38,59} H can passivate dangling bonds, removing those defects from the band gap. These defects are always the lowest-energy configuration and in essence represent a healing of the network via the removal of undercoordinated centers. Their formation energies are negative with the chemical potential convention employed here and are thus favored regardless of the starting geometry. It is important to note that while energetically favored, the concentration of passivation sites is limited by the number of dangling bonds present in the pristine cell used for this study.

The insertion of H across strained Si–N bonds is found to provide a route for H-induced defect formation and disruption of the amorphous network. It constitutes an important atomistic mechanism for the experimentally observed H-induced softening of a-Si₃N₄.^{23,43,44} While having some similarities with the H-induced bond rupture seen in SiO₂, there are some important differences, with Si–H formation being favored as opposed to N-centered H defects. Both in our study and within a realistic a-Si₃N₄ film, H insertion is naturally limited by the number of strained precursor sites. The further implication is that the strain present in the film as a result of the substrate or growth conditions will directly impact the H_{ins} concentration by influencing the number of precursor sites. The same argument can be extended to the distribution of precursor sites within a given film, with more strained environments found in close proximity to the a-Si₃N₄–substrate interface(s) within a device stack.

A majority of H defects interact with N/Si with intact coordination shells and sit in a broad range of formation energies with the H_{i-N} ($E_f^0 = 1.81$ eV) centers typically lower in energy than H_{i-Si} and H_{bri} ($E_f^0 = 2.18$ eV). The range of energy is largely dictated by the steric environment of the reference atom in the pristine state before H incorporation. Perhaps most intriguingly, the CTLs sit in a narrow range for each of the main classes of H defects for both centers (H_{i-N}, H_{i-Si}, and H_{ins}). This very small spread of the CTLs across a range of defect configurations in stark contrast to their formation energetics seems puzzling at first glance. An examination of the nature of the defect states reveals the reason: in each case, the H configuration is independent of the charge state. This is driven by the H states sitting deep within the valence (and conduction) bands, thereby playing no active role in charge trapping. Instead, they merely act as carriers of an initial electron or hole localizing in a charge trap state predetermined by pristine a-Si₃N₄, i.e., at the h^+ and e^- trap sites we have identified in our previous work.⁵⁸ This is schematically summarized in Table 1.

We now compare H incorporation in a-Si₃N₄ to that of the much more widely studied oxide system. Here, H forms

amphoteric defects whose charge states are dictated by the Fermi energy with the (+/–) CTLs sitting approximately 4.25 eV below the vacuum level.^{48,51} In contrast, H incorporation in a-Si₃N₄ is quite different, where the localized nature of the band edges and the propensity for the system to trap electrons and holes result in a charging of the a-Si₃N₄ dielectric layer. In common with a-SiO₂, H in a-Si₃N₄ is found to facilitate the breaking of strained bonds. However, the mechanisms are quite different: rather than creating an analog of the hydroxylated E',⁵³ H preferentially adds to the Si site in the first instance. It is equally important to note that in the case of a-SiO₂ the charge trapping occurs at the center where the bond breaks, whereas in a-Si₃N₄ the charge is located on a trap site unrelated to the site of H insertion.

At this juncture, it is important to raise two questions that go beyond the scope of this work. First, how is H incorporation affected in Si- and N-rich Si_xN_y? This is important because tuning the stoichiometry is used to achieve the application-specific performance of the material. In cases where deviations from stoichiometric a-Si₃N₄ are small, it would be reasonable to expect behavior similar to that described here. However, when the deviations are significant, new structural motifs might be introduced that are not captured by the present study. Second, how do the nature of the intrinsic trap sites and the range of levels previously described⁵⁸ affect H incorporation? Both of these questions together with the impact of increasing the H concentration are currently under investigation.

In summary, our investigation of H defect centers in a-Si₃N₄ uncovers the multifaceted role of H. While hydrogen has been known to passivate dangling bonds, thereby enhancing the electronic and optical properties playing the role of “Jekyll”, beyond passivation, its “Hyde” also emerges: incorporated H atoms instigate Si–N bond disruptions, especially in strained regions characterized by a distorted Si coordination environment and at least one elongated Si–N bond. It is noteworthy that a majority of hydrogen-associated states, whether from NH or most SiH configurations, reside within the valence and conduction bands, rendering them electronically inert. Charge trapping is predominantly linked to intrinsic traps for NH defects and N centers (or two-coordinate N) in the case of SiH defects, although a few high-energy H configurations act as exceptions. The identification of an intrinsic electron bipolaron in the –1 charge state for NH defects, which induces a significant relaxation in the amorphous network, requires further study. Importantly, this study bridges the understanding between H behavior in a-SiO₂ and a-Si₃N₄ while emphasizing some important differences. It is plausible to infer, and left for future work to be confirmed, that analogous behavior could be seen in materials characterized by band edges that show a degree of localization.

COMPUTATIONAL METHODS

Fermi energy and charge-dependent defect formation energies $E_{\text{form}}(E_F; q)$ for the incorporation of hydrogen into a-Si₃N₄ were calculated using the standard formalism of Zhang and Northrup⁶³ based on density functional theory (DFT) at the hybrid functional level. The chemical potential of H has been taken as $\frac{1}{2}$ H₂. In the following, defect formation energies for the incorporation of hydrogen in the neutral charge state ($E_f^0 = E_{\text{form}}(E_F; 0)$) are generally referred to as the formation energies. By convention, the charge transition level (CTL) is defined as the Fermi energy at which the formation energy of two charge

states is equal ($E_{\text{form}}(q) - E_{\text{form}}(q') = 0$). Finite-size corrections for the charged systems are performed using the Lany–Zunger correction scheme.⁶⁴ All DFT calculations were performed spin-polarized with the CP2K⁶⁵ code using the HSE06^{66,67} exchange–correlation functional with the auxiliary density matrix method (ADMM).⁶⁸ The DZVP-SR-MOLOPT⁶⁹ family of basis sets was employed to describe the valence electrons together with GTH pseudopotentials^{70–72} for the core electrons. More computational details are provided in the [Supporting Information](#).

The problem of structure sampling was explored at length in our previous work as it represents a vital consideration for amorphous systems.⁵⁸ A single α - Si_3N_4 cell is selected to allow the problem of site sampling to be untangled from the broad range of intrinsic trap sites previously described. To achieve this, the previous statistical sampling scheme is extended to the consideration of H defects, capturing the variety of geometries of the host lattice. These results are included in the [Supporting Information](#) and result in the selection of 60 seed sites for H incorporation, with 25 (35) originally centered at Si (N), respectively.

■ ASSOCIATED CONTENT

Data Availability Statement

All structures generated in this study are available via zenodo.org (10.5281/zenodo.10054617), together with input parameters and specifications for the compilation of the CP2K package.

Supporting Information

The Supporting Information is available free of charge at <https://pubs.acs.org/doi/10.1021/acs.jpcllett.3c03376>.

More computational details; hydrogen incorporation in β - Si_3N_4 ; properties of the pristine cell; statistical sampling of hydrogen incorporation sites; additional characterization of structural effects; and hydrogen-induced trap sites ([PDF](#))

■ AUTHOR INFORMATION

Corresponding Author

Jörg Meyer – *Leiden Institute of Chemistry, Gorlaeus Laboratories, Leiden University, 2300 RA Leiden, The Netherlands*; orcid.org/0000-0003-0146-730X; Email: j.meyer@chem.leidenuniv.nl

Authors

Jonathon Cottom – *Leiden Institute of Chemistry, Gorlaeus Laboratories, Leiden University, 2300 RA Leiden, The Netherlands*; orcid.org/0000-0002-5918-9464

Lukas Hückmann – *Leiden Institute of Chemistry, Gorlaeus Laboratories, Leiden University, 2300 RA Leiden, The Netherlands*; orcid.org/0000-0003-4718-4604

Emilia Olsson – *Advanced Research Center for Nanolithography, 1098 XG Amsterdam, The Netherlands; Institute for Theoretical Physics, University of Amsterdam, 1090 GL Amsterdam, The Netherlands*

Complete contact information is available at <https://pubs.acs.org/doi/10.1021/acs.jpcllett.3c03376>

Notes

The authors declare no competing financial interest.

■ ACKNOWLEDGMENTS

This research is cofinanced by Holland High Tech through a public–private partnership in research and development within the Dutch top sector of High-Tech Systems and Materials (HTSM). This work used the Dutch national e-infrastructure with the support of the SURF Cooperative using grant nos. EINF-3219, EINF-4531, EINF-5451, and EINF-5872. E.O. is grateful for a WISE Fellowship from the Dutch Research Council (NWO). Part of this work has been carried out at the Advanced Research Center for Nanolithography (ARCNL). ARCNL is a public–private partnership with founding partners UvA, VU, NWO-I, and ASML and associate partner RUG.

■ REFERENCES

- (1) Okada, A. Automotive and industrial applications of structural ceramics in Japan. *J. Eur. Ceram. Soc.* **2008**, *28*, 1097–1104.
- (2) Doo, V. Y.; Nichols, D. R.; Silvey, G. A. Preparation and properties of pyrolytic silicon nitride. *J. Electrochem. Soc.* **1966**, *113*, 1279.
- (3) Tsai, S.-J.; Wang, C.-L.; Lee, H.-C.; Lin, C.-Y.; Chen, J.-W.; Shiu, H.-W.; Chang, L.-Y.; Hsueh, H.-T.; Chen, H.-Y.; Tsai, J.-Y.; et al. Approaching defect-free amorphous silicon nitride by plasma-assisted atomic beam deposition for high performance gate dielectric. *Sci. Rep.* **2016**, *6*, No. 28326.
- (4) Törmä, P. T.; Sipilä, H. J.; Mattila, M.; Kostamo, P.; Kostamo, J.; Kostamo, E.; Lipsanen, H.; Nelms, N.; Shortt, B.; Bavdaz, M.; et al. Ultra-thin silicon nitride X-ray windows. *IEEE Trans. Nucl. Sci.* **2013**, *60*, 1311–1314.
- (5) Törmä, P. T.; Kostamo, J.; Sipilä, H.; Mattila, M.; Kostamo, P.; Kostamo, E.; Lipsanen, H.; Laubis, C.; Scholze, F.; Nelms, N.; et al. Performance and Properties of Ultra-Thin Silicon Nitride X-ray Windows. *IEEE Trans. Nucl. Sci.* **2014**, *61*, 695–699.
- (6) Cornaby, S.; Bilderback, D. H. Silicon nitride transmission X-ray mirrors. *J. Synch. Rad.* **2008**, *15*, 371–373.
- (7) Sharma, T.; Wang, J.; Kaushik, B. K.; Cheng, Z.; Kumar, R.; Wei, Z.; Li, X. Review of recent progress on silicon nitride-based photonic integrated circuits. *IEEE Access* **2020**, *8*, 195436–195446.
- (8) Xiang, C.; Jin, W.; Bowers, J. E. Silicon nitride passive and active photonic integrated circuits: trends and prospects. *Photon. Res.* **2022**, *10*, A82–A96.
- (9) Goldfarb, D. L. Fabrication of a full-size EUV pellicle based on silicon nitride. *SPIE Photomask Technology* **2015**, 9635, 96350A.
- (10) Pollentier, I.; Lee, J. U.; Timmermans, M.; Adelman, C.; Zahedmanesh, H.; Huyghebaert, C.; Gallagher, E. E. Novel membrane solutions for the EUV pellicle: better or not? *Extreme Ultraviolet (EUV) Lithography VIII*; SPIE: 2017; p 101430L.
- (11) van de Kerkhof, M.; Yakunin, A. M.; Kvon, V.; Nikipelov, A.; Astakhov, D.; Krainov, P.; Banine, V. EUV-induced hydrogen plasma and particle release. *Radiat. Eff. Defect. S.* **2022**, *177*, 486–512.
- (12) Zhang, J.; Liu, G.; Cui, W.; Ge, Y.; Du, S.; Gao, Y.; Zhang, Y.; Li, F.; Chen, Z.; Du, S.; et al. Plastic deformation in silicon nitride ceramics via bond switching at coherent interfaces. *Science* **2022**, *378*, 371–376.
- (13) Liu, N.; Yang, X.; Zhu, Z.; Chen, F.; Zhou, Y.; Xu, J.; Liu, K. Silicon nitride waveguides with directly grown WS₂ for efficient second-harmonic generation. *Nanoscale* **2021**, *14*, 49–54.
- (14) Aiyama, T.; Fukunaga, T.; Niihara, K.; Hirai, T.; Suzuki, K. An X-ray diffraction study of the amorphous structure of chemically vapor-deposited silicon nitride. *J. Non-Cryst. Solids* **1979**, *33*, 131–139.
- (15) Misawa, M.; Fukunaga, T.; Niihara, K.; Hirai, T.; Suzuki, K. Structure characterization of CVD amorphous Si_3N_4 by pulsed neutron total scattering. *J. Non-Cryst. Solids* **1979**, *34*, 313–321.
- (16) Wakita, K.; Hayashi, H.; Nakayama, Y. Structural study of amorphous SiN_x : H films produced by plasma-enhanced chemical vapor deposition. *Jpn. J. Appl. Phys.* **1996**, *35*, 2557.
- (17) Deshpande, S. V.; Gulari, E.; Brown, S. W.; Rand, S. C. Optical properties of silicon nitride films deposited by hot filament chemical vapor deposition. *J. Appl. Phys.* **1995**, *77*, 6534–6541.

- (18) Sahu, B. S.; Delachat, F.; Slaoui, A.; Carrada, M.; Ferblantier, G.; Muller, D. Effect of annealing treatments on photoluminescence and charge storage mechanism in silicon-rich $\text{SiN}_x\text{:H}$ films. *Nanoscale Res. Lett.* **2011**, *6*, 178.
- (19) Gritsenko, V.; Kruchinin, V.; Prosvirin, I.; Novikov, Y. N.; Chin, A.; Volodin, V. Atomic and electronic structures of a- $\text{SiN}_x\text{:H}$. *J. Exp. Theor. Phys.* **2019**, *129*, 924–934.
- (20) Robertson, J. Defect densities and hydrogen diffusion in hydrogenated amorphous Si-based alloys. *Appl. Phys. Lett.* **1991**, *59*, 3425–3427.
- (21) Warren, W. L.; Robertson, J.; Kanicki, J. Si and N dangling bond creation in silicon nitride thin films. *Appl. Phys. Lett.* **1993**, *63*, 2685–2687.
- (22) Krick, D. T.; Lenahan, P. M.; Kanicki, J. Nature of the dominant deep trap in amorphous silicon nitride. *Phys. Rev. B* **1988**, *38*, 8226–8229.
- (23) Hasegawa, S.; Amano, Y.; Inokuma, T.; Kurata, Y. Effects of active hydrogen on the stress relaxation of amorphous $\text{SiN}_x\text{:H}$ films. *J. Appl. Phys.* **1994**, *75*, 1493–1500.
- (24) Martinez, F. L.; del Prado, A.; Martil, I.; Gonzalez-Diaz, G.; Selle, B.; Sieber, I. Thermally induced changes in the optical properties of $\text{SiN}_x\text{:H}$ films deposited by the electron cyclotron resonance plasma method. *J. Appl. Phys.* **1999**, *86*, 2055–2061.
- (25) Roizin, Y. Failure phenomena due to hydrogen migration in amorphous a- $\text{SiN}_x\text{:H}$ films. *J. Non-Cryst. Solids* **1991**, *137–138*, 61–64.
- (26) Bommali, R. K.; Ghosh, S.; Vijaya Prakash, G.; Gao, K.; Zhou, S.; Khan, S. A.; Srivastava, P. Hydrogen plasma induced modification of photoluminescence from a- $\text{SiN}_x\text{:H}$ thin films. *J. Appl. Phys.* **2014**, *115*, No. 053525.
- (27) Zoldesi, C.; Bal, K.; Blum, B.; Bock, G.; Brouns, D.; Dhalluin, F.; Dzionkina, N.; Espinoza, J. D. A.; de Hoogh, J.; Houweling, S. et al. *Progress on EUV Pellicle Development. Extreme Ultraviolet (EUV) Lithography V*; SPIE: 2014; p 90481N.
- (28) Warren, W. L.; Lenahan, P. M. Electron-nuclear double-resonance and electron-spin-resonance study of silicon dangling-bond centers in silicon nitride. *Phys. Rev. B* **1990**, *42*, 1773–1780.
- (29) Warren, W. L.; Lenahan, P. M.; Curry, S. E. First observation of paramagnetic nitrogen dangling-bond centers in silicon nitride. *Phys. Rev. Lett.* **1990**, *65*, 207–210.
- (30) Warren, W.; Kanicki, J.; Rong, F.; Poindexter, E. Paramagnetic Point Defects in Amorphous Silicon Dioxide and Amorphous Silicon Nitride Thin Films: II. *J. Electrochem. Soc.* **1992**, *139*, 880.
- (31) Warren, W.; Robertson, J.; Kanicki, J. Si and N dangling bond creation in silicon nitride thin films. *Appl. Phys. Lett.* **1993**, *63*, 2685–2687.
- (32) Warren, W. L.; Kanicki, J.; Poindexter, E. H. Paramagnetic point defects in silicon nitride and silicon oxynitride thin films on silicon. *Colloids Surf. A Physicochem. Eng. Asp.* **1996**, *115*, 311–317.
- (33) Di Valentin, C.; Palma, G.; Pacchioni, G. Ab initio study of transition levels for intrinsic defects in silicon nitride. *J. Phys. Chem. C* **2011**, *115*, 561–569.
- (34) Hintzsche, L.; Fang, C.; Watts, T.; Marsman, M.; Jordan, G.; Lamers, M.; Weeber, A.; Kresse, G. Density functional theory study of the structural and electronic properties of amorphous silicon nitrides: $\text{Si}_3\text{N}_{4-x}\text{:H}$. *Phys. Rev. B* **2012**, *86*, No. 235204.
- (35) Kroll, P. Structure and reactivity of amorphous silicon nitride investigated with density-functional methods. *J. Non-Cryst. Solids* **2001**, *293–295*, 238–243.
- (36) Choi, W. I.; Son, W.-J.; Dronskowski, R.; Oh, Y.; Yang, S.-Y.; Kwon, U.; Kim, D. S. Switchable chemical-bond reorganization for the stable charge trapping in amorphous silicon nitride. *Adv. Mater.* **2023**, *2308054*, DOI: 10.1002/adma.202308054.
- (37) Rehman, A.; van de Kruijs, R. W. E.; van den Beld, W. T. E.; Sturm, J. M.; Ackermann, M. Chemical interaction of hydrogen radicals (H^*) with transition metal nitrides. *J. Phys. Chem. C* **2023**, *127*, 17770–17780.
- (38) Wilhelmer, C.; Waldhoer, D.; Milardovich, D.; Cvitkovich, L.; Waltl, M.; Grasser, T. Intrinsic Electron Trapping in Amorphous Silicon Nitride (a- $\text{Si}_3\text{N}_4\text{:H}$). 2023 *International Conference on Simulation of Semiconductor Processes and Devices (SISPAD)*; IEEE: 2023; pp 149–152.
- (39) Mártil, I.; del Prado, A.; San Andrés, E.; González Díaz, G.; Martínez, F. L. Rapid thermally annealed plasma deposited $\text{SiN}_x\text{:H}$ thin films: Application to metal–insulator–semiconductor structures with Si, $\text{In}_{0.53}\text{Ga}_{0.47}\text{As}$, and InP . *J. Appl. Phys.* **2003**, *94*, 2642–2653.
- (40) San Andrés, E.; Del Prado, A.; Martínez, F.; Mártil, I.; Bravo, D.; López, F. Rapid thermal annealing effects on the structural properties and density of defects in SiO_2 and $\text{SiN}_x\text{:H}$ films deposited by electron cyclotron resonance. *J. Appl. Phys.* **2000**, *87*, 1187–1192.
- (41) Warren, W. L.; Kanicki, J.; Robertson, J.; Poindexter, E. H.; McWhorter, P. J. Electron paramagnetic resonance investigation of charge trapping centers in amorphous silicon nitride films. *J. Appl. Phys.* **1993**, *74*, 4034–4046.
- (42) Song, C.; Huang, R.; Wang, X.; Guo, Y.; Song, J.; Zhang, Y.; Zheng, Z. Effects of hydrogen on photoluminescence properties of a- $\text{SiN}_x\text{:H}$ films prepared by VHF-PECVD. *Appl. Surf. Sci.* **2011**, *258*, 1290–1293.
- (43) Lindley, M.; Elias, D.; Jones, B.; Pitman, K. The influence of hydrogen in the nitriding gas on the strength, structure and composition of reaction-sintered silicon nitride. *J. Mater. Sci.* **1979**, *14*, 70–85.
- (44) Laarz, E.; Zhmud, B. V.; Bergström, L. Dissolution and deagglomeration of silicon nitride in aqueous medium. *J. Am. Ceram. Soc.* **2000**, *83*, 2394–400.
- (45) Van de Walle, C. G.; Denteneer, P. J. H.; Bar-Yam, Y.; Pantelides, S. T. Theory of hydrogen diffusion and reactions in crystalline silicon. *Phys. Rev. B* **1989**, *39*, 10791–10808.
- (46) Neugebauer, J.; Van de Walle, C. G. Hydrogen in GaN: Novel aspects of a common impurity. *Phys. Rev. Lett.* **1995**, *75*, 4452–4455.
- (47) Van de Walle, C. G. Hydrogen as a cause of doping in zinc oxide. *Phys. Rev. Lett.* **2000**, *85*, 1012–1015.
- (48) Van de Walle, C. G.; Neugebauer, J. Universal alignment of hydrogen levels in semiconductors, insulators and solutions. *Nature* **2003**, *423*, 626–628.
- (49) Robertson, J.; Peacock, P. Doping and hydrogen in wide gap oxides. *Thin Solid Films* **2003**, *445*, 155–160.
- (50) Xiong, K.; Robertson, J.; Clark, S. J. Behavior of hydrogen in wide band gap oxides. *J. Appl. Phys.* **2007**, *102*, No. 083710.
- (51) Li, H.; Robertson, J. Behaviour of hydrogen in wide band gap oxides. *J. Appl. Phys.* **2014**, *115*, No. 203708.
- (52) Godet, J.; Pasquarello, A. Ab initio study of charged states of H in amorphous SiO_2 . *Microelectron. Eng.* **2005**, *80*, 288–291.
- (53) El-Sayed, A.-M.; Watkins, M. B.; Grasser, T.; Afanas'ev, V. V.; Shluger, A. L. Hydrogen-induced rupture of strained Si-O bonds in amorphous silicon dioxide. *Phys. Rev. Lett.* **2015**, *114*, No. 115503.
- (54) El-Sayed, A.-M.; Wimmer, Y.; Goes, W.; Grasser, T.; Afanas'ev, V. V.; Shluger, A. L. Theoretical models of hydrogen-induced defects in amorphous silicon dioxide. *Phys. Rev. B* **2015**, *92*, No. 014107.
- (55) Wilhelmer, C.; Waldhoer, D.; Jech, M.; El-Sayed, A.-M. B.; Cvitkovich, L.; Waltl, M.; Grasser, T. Ab initio investigations in amorphous silicon dioxide: Proposing a multi-state defect model for electron and hole capture. *Microelectron Reliab* **2022**, *139*, No. 114801.
- (56) Griggs, D. Hydrolytic weakening of quartz and other silicates. *Geophys. J. Int.* **1967**, *14*, 19–31.
- (57) Herrmann, M. Corrosion of silicon nitride materials in aqueous solutions. *J. Am. Ceram. Soc.* **2013**, *96*, 3009–3022.
- (58) Hückmann, L.; Cottom, J.; Meyer, J. Intrinsic charge trapping and reversible charge induced structural modifications in a- Si_3N_4 . *Adv. Phys. Res.* **2023**, No. 2300109.
- (59) Grillo, M.-E.; Elliott, S. D.; Freysoldt, C. Native defects in hexagonal $\beta\text{-Si}_3\text{N}_4$ studied using density functional theory calculations. *Phys. Rev. B* **2011**, *83*, No. 085208.
- (60) Martin, J. M. L.; Lee, T. J.; Taylor, P. R. An accurate ab initio quartic force field for ammonia. *J. Chem. Phys.* **1992**, *97*, 8361–8371.
- (61) Boyd, D. R. J. Infrared spectrum of triethylsilane and the structure of the silane molecule. *J. Chem. Phys.* **1955**, *23*, 922–926.

(62) Wimmer, Y.; El-Sayed, A.-M.; Gös, W.; Grasser, T.; Shluger, A. L. Role of hydrogen in volatile behaviour of defects in SiO₂-based electronic devices. *Proc. Math. Phys. Eng. Sci.* **2016**, *472*, No. 20160009.

(63) Zhang, S. B.; Northrup, J. E. Chemical potential dependence of defect formation energies in GaAs: Application to Ga self-diffusion. *Phys. Rev. Lett.* **1991**, *67*, 2339–2342.

(64) Lany, S.; Zunger, A. Accurate prediction of defect properties in density functional supercell calculations. *Model. Simul. Mater. Sci. Eng.* **2009**, *17*, No. 084002.

(65) Kühne, T. D.; Iannuzzi, M.; Del Ben, M.; Rybkin, V. V.; Seewald, P.; Stein, F.; Laino, T.; Khaliullin, R. Z.; Schütt, O.; Schiffmann, F.; et al. CP2K: An electronic structure and molecular dynamics software package - Quickstep: Efficient and accurate electronic structure calculations. *J. Chem. Phys.* **2020**, *152*, No. 194103.

(66) Heyd, J.; Scuseria, G. E.; Ernzerhof, M. Hybrid functionals based on a screened Coulomb potential. *J. Chem. Phys.* **2003**, *118*, 8207–8215.

(67) Heyd, J.; Scuseria, G. E.; Ernzerhof, M. Erratum: “Hybrid functionals based on a screened Coulomb potential. *J. Chem. Phys.* **2003**, *118*, 8207.

(68) Guidon, M.; Hutter, J.; VandeVondele, J. Auxiliary density matrix methods for Hartree-Fock exchange calculations. *J. Chem. Theor. and Comp.* **2010**, *6*, 2348–2364.

(69) VandeVondele, J.; Hutter, J. Gaussian basis sets for accurate calculations on molecular systems in gas and condensed phases. *J. Chem. Phys.* **2007**, *127*, No. 114105.

(70) Goedecker, S.; Teter, M.; Hutter, J. Separable dual-space Gaussian pseudopotentials. *Phys. Rev. B* **1996**, *54*, 1703–1710.

(71) Hartwigsen, C.; Goedecker, S.; Hutter, J. Relativistic separable dual-space Gaussian pseudopotentials from H to Rn. *Phys. Rev. B* **1998**, *58*, 3641–3662.

(72) Krack, M. Pseudopotentials for H to Kr optimized for gradient-corrected exchange-correlation functionals. *Theor. Chem. Acc.* **2005**, *114*, 145–152.